Inorganic Chemistry Article

Inorg. Chem. 2010, 49, 9949–9957 9949
DOI: 10.1021/ic101216z

Contrasts in Structural and Bonding Representations among Polar Intermetallic Compounds. Strongly Differentiated Hamilton Populations for Three Related Condensed Cluster Halides of the Rare-Earth Elements

Shalabh Gupta,[†] Gerd Meyer,[§] and John D. Corbett*[,‡]

[†] *Ames Laboratory, and* [‡] *Department of Chemistry, Iowa State University, Ames, Iowa 50011, and*
[§] *Department of Chemistry, Universität zu Köln, Köln 50939, Germany*

Received June 21, 2010

The crystal and electronic structures of three related R_3TnX_3 phases (R = rare-earth metal, Tn = transition metal, X = Cl, I) containing extended mixed-metal chains are compared and contrasted: (**1**) Pr_3RuI_3 ($P2_1/m$), (**2**) Gd_3MnI_3 ($P2_1/m$), and (**3**) Pr_3RuCl_3 (*Pnma*). The structures all feature double chains built of pairs of condensed R_6(Tn) octahedral chains encased by halogen atoms. Pr_3RuI_3 (**1**) lacks significant Ru−Ru bonding, evidently because of packing restrictions imposed by the large closed-shell size of iodine. However, the vertex Pr2 atoms on the chain exhibit a marked electronic differentiation. These are strongly bound to the central Ru (and to four I), but very little to four neighboring Pr in the cluster according to bond populations, in contrast to Pr2−Pr "bond" distances that are very comparable to those elsewhere. In Gd_3MnI_3 (**2**), the smaller metal atoms allow substantial distortions and Mn−Mn bonding. Pr_3RuCl_3 (**3**), in contrast to the iodide (**1**), can be described in terms of a more tightly bound superstructure of (**2**) in which both substantial Ru−Ru bonding and an increased number of Pr−Cl contacts in very similar mixed-metal chains are favored by the smaller closed-shell contacts of chlorine. Local Spin Density Approximation (LSDA) Linearized Muffin-Tin Orbital (LMTO)-ASA calculations and Crystal Orbital Hamilton Population (COHP) analyses show that the customary structural descriptions in terms of condensed, Tn-stuffed, R−R bonded polyhedral frameworks are poor representations of the bonding in all. Hamilton bond populations (−ICOHP) for the polar mixed-metal R−Tn and the somewhat smaller R−X interactions account for 75−90% of the total populations in each of these phases, together with smaller contributions and variations for R−R and Tn−Tn interactions. The strength of such R−Tn contributions in polar intermetallics was first established or anticipated by Brewer. The rare-earth-metal atoms are significantly oxidized in these compounds.

Introduction

The present investigation was prompted by the results of recent studies on the opposed type of relatively electron-poor Zintl phases: polar intermetallics that form when earlier main group s or p (or late transition metal d) elements are substituted into normal Zintl phases.[1] Classical examples of the last typically contain active (alkali A, alkaline-earth Ae) metals combined with main-group 14−16 p-elements such that polyanionic bonding in the structures follows octet (closed shell) rules, which lead in principle to semiconducting or insulating valence compounds.[2] Substitutions of earlier electron-poorer elements in these (beyond some threshold) generally yield metallic cluster phases with higher atomic coordination numbers and more extended bonding.[3]

Recent studies show that, relative to more classical motifs, many new and remarkable 2D and 3D structural variations appear among such polar intermetallics, particularly when heavy late transition metals (Tn) are bound with main-group p-metals, as for the new K_3Au_5In,[4] $K_{12}Au_{21}Sn_4$,[5] $BaAuIn_3$,[6] Sr_2Pt_2In,[7] Ca_3Au_3In,[8] $BaHg_2Tl_2$,[9] and $CaAu_4Bi$.[10] Linearized muffin-tin orbital (LMTO)-ASA density functional theory (DFT) calculations on these have provided useful and provocative information regarding the structures and their bonding, allowing better assessments of relative bonding

---

*To whom correspondence should be addressed. E-mail: jcorbett@iastate.edu.

(1) Corbett, J. D. *Inorg. Chem.* **2010**, *49*, 13.
(2) Kauzlarich, S., Ed.; *Chemistry, Structure and Bonding of Zintl Phases and Ions*; VCH Publishers: New York, 1996.
(3) Corbett, J. D. *Angew. Chem., Int. Ed.* **2000**, *39*, 670.
(4) Li, B.; Kim, S.-J.; Miller, G. J.; Corbett, J. D. *Inorg. Chem.* **2009**, *48*, 6573.
(5) Li, B.; Kim, S.-J.; Miller, G. J.; Corbett, J. D. *Inorg. Chem.* **2009**, *48*, 11108.
(6) Liu, S.; Corbett, J. D. *Inorg. Chem.* **2004**, *43*, 4988.
(7) Muts, I. R.; Nilges, T.; Rodewald, U. C.; Zaremba, V. I.; Pöttgen, R. *Z. Naturforsch. B.* **2007**, *62*, 56.
(8) Muts, I. R.; Zaremba, V. I.; Rodewald, U. C.; Pöttgen, R. *Z. Anorg. Allg. Chem.* **2008**, *63*, 848.
(9) Dai, J.-C.; Gupta, S.; Gourdon, O.; Kim, H.-J.; Corbett, J. D. *J. Am. Chem. Soc.* **2009**, *131*, 8677.
(10) Lin, Q.; Corbett, J. D. *J. Am. Chem. Soc.* **2010**, *132*, 5662.

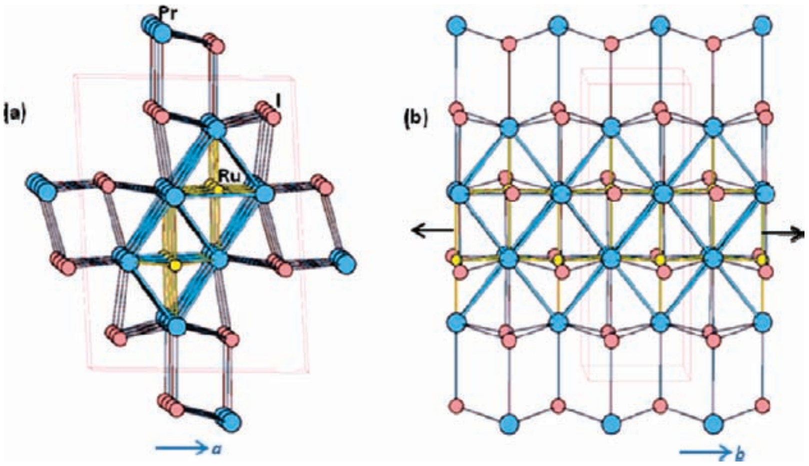

Figure 1. Unit cell of Pr_3RuI_3 ($P2_1/m$) with an alternate origin choice for clarity. (a) A single Pr_6Ru_2 chain and all bridging iodine as viewed in projection along the short b axis; (b) A side [100] view of a portion of a single chain (horizontal). (Pr is blue, Ru yellow, I light salmon). Note that successive shared $Pr_{6/2}(Ru)$ octahedra alternate in depth in both (a) and (b).

contributions of different atom-pair interactions, particularly in terms of the more meaningful COHP (Crystal Orbital Hamilton Population) functions and their energy-weighted population sums −ICOHP.[11,12] Especially noteworthy have been the major but evidently unappreciated effects that late 4d and 5d elements (Tn) have on Tn−Tn, the more polar Tn−p-element, and even A−Tn bond populations. Extended metal−metal interactions and relatively delocalized bonding that lack any sense of conventional valence rules can be better understood with the aid of such theoretical descriptions.

These developments have piqued our interests in bonding systematics among the longer-known inverse[1] type of intermetallic cluster phases, the novel ternary rare-earth-metal (R) cluster halides (X = Cl, Br, I) or tellurides in which late transition metals (Tn) center relatively electron-poor, isolated or condensed octahedral $R_6(Tn)$ or related cluster units.[13−16] In these cases, individual idealized X^- or Te^{2-} counterparts of the foregoing cations now occupy cavities between the mixed R−Tn cationic networks. Early bonding considerations suggested that the Tn members generally contribute additional electrons as well as strong polar R−Tn bonding interactions.[17,18] One particularly interesting and tractable family of ternary R−Tn−(X,Te) phases exhibit related infinite 1-, 2-, or 3-dimensional arrays of condensed clusters, but their theoretical considerations have substantially been only at the extended-Hückel level. We give here new descriptions and analyses of the geometric and bonding aspects for three R_3TnX_3-type phases with 1-D mixed metal chain structures, phases that have been reported and discussed separately over an 18-year period, namely, Pr_3RuI_3,[19] Gd_3MnI_3,[20] and Pr_3RuCl_3.[21] These occur in the same monoclinic space group $P2_1/m$ or an orthorhombic $Pnma$ supergroup thereof, and their diverse structures can all be newly described in terms of closely related condensed octahedral clusters. Computational analyses of these in terms of COHP and −ICOHP data for the R−R, R−Tn, Tn−Tn, and R−X interactions reveal that the dominant population (bonding) contributions in all three come from the polar R−Tn and R−X components, in contrast to the R−R cluster interactions that experimentalists have commonly featured in their structure descriptions. Conversely, important bonding features and differences among the members of this series cannot be discerned from specific structural features alone. Calculational details are summarized in the Supporting Information.

Results and Discussion

Pr_3RuI_3. The basically undistorted limit in a diverse group of R_3TnI_3 compositions[19] is represented by Pr_3RuI_3, illustrated in Figure 1 by means of (a) the [010] projection down the short (~4.28 Å) b axis, and (b) a [100] side view of a section of a single metal chain and its bonded iodines. (All atoms lie on mirror planes at $y = 0$ or 1/2.) Conceptually, the doubly condensed structural motif can be generated from two parallel metal chains, each built of $Pr_6(Ru)$ octahedra that share trans-edges (as in Pr_4RuI_5[22]). The two chains, displaced from each other by half the chain repeat (b), are then condensed side-by-side through shared Pr−Pr side edges so as to generate double chains. The multifunctional I atoms around the central double chain in (a) cap Pr_3 faces, bridge Pr_2 edges, and bond exo at single Pr vertexes on either a single or adjoining chains so as to generate the infinite structure in the a−b plane. The iodines are 3-, 4-, or 5-bonded to R, which might suggest (correctly) that full R−I bonding capabilities are not being realized. In the simplest view, the iodine sheath has often been assumed to preclude further R−R condensation. On the other hand, the Ru−Ru interactions are relatively weak owing to their

---

[11] Dronskowski, R.; Blöchl, P. *J. Phys. Chem.* **1993**, *97*, 8617.

[12] Dronskowski, R. *Computational Chemistry of Solid State Materials*; Wiley-VCH Verlag: Weinheim, Germany, 2005; p 92.

[13] Corbett, J. D. *J. Alloys Compd.* **2006**, *418*, 1.

[14] Corbett, J. D. In *Inorganic Chemistry in Focus II*; Meyer, G., Naumann, D., Wesemann, L., Eds.; Wiley-VCH: Weinheim, Germany, 2005; Vol. *2*, Chapter 8.

[15] Herzmann, N.; Gupta, S.; Corbett, J. D. *Z. Anorg. Allg. Chem.* **2009**, *635*, 848.

[16] Meyer, G. *Z. Anorg. Allg. Chem.* **2008**, *634*, 2729.

[17] Hughbanks, T.; Rosenthal, G.; Corbett, J. D. *J. Am. Chem. Soc.* **1988**, *110*, 1511.

[18] Brewer, L.; Wengert, P. R. *Metall. Trans* **1973**, *4*, 83.

[19] Payne, M. W.; Dorhout, P. K.; Kim, S.-J.; Hughbanks, T. R.; Corbett, J. D. *Inorg. Chem.* **1992**, *31*, 1389.

[20] Ebihara, M.; Martin, J. D.; Corbett, J. D. *Inorg. Chem.* **1994**, *33*, 2079.

[21] Herzmann, N.; Mudring, A.-V.; Meyer, G. *Inorg. Chem.* **2008**, *47*, 7954.

[22] Payne, M. W.; Dorhout, P. K.; Corbett, J. D. *Inorg. Chem.* **1991**, *30*, 1467.

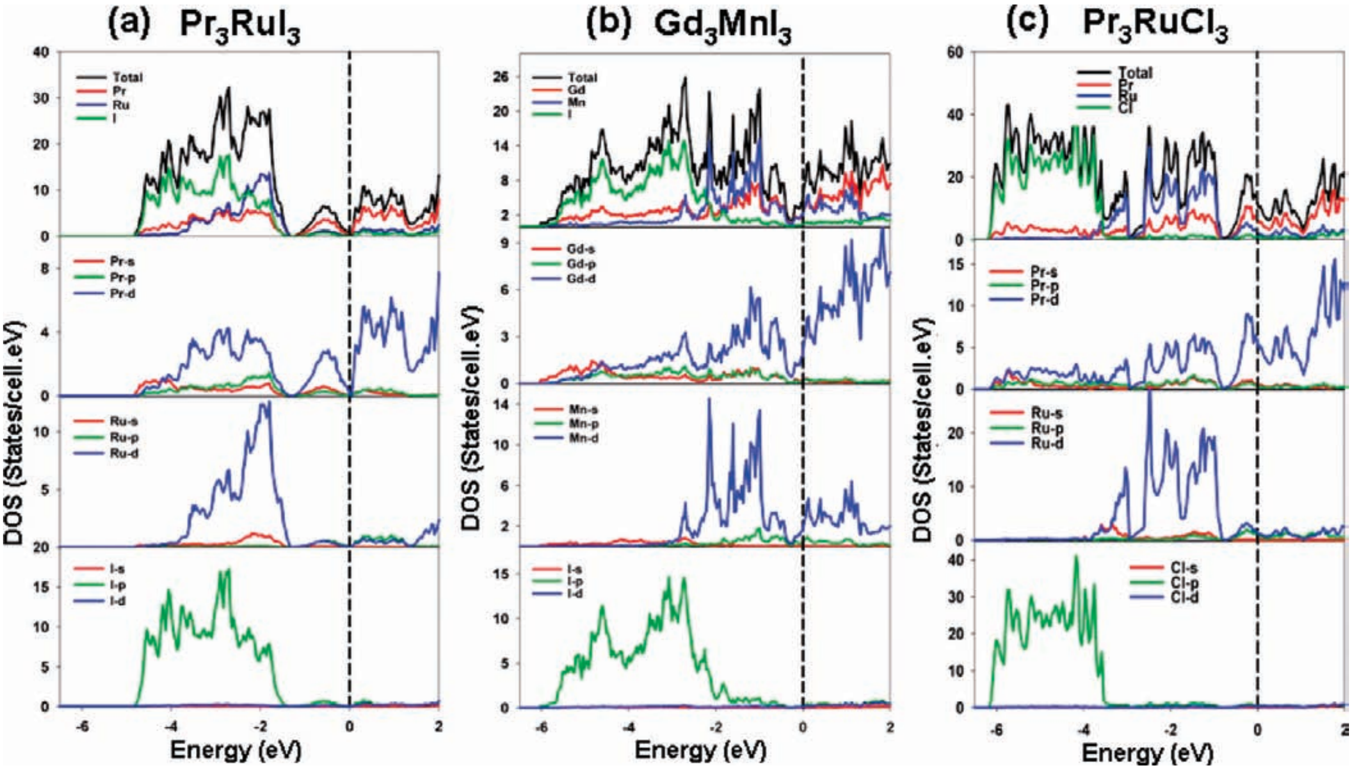

Figure 2. Total DOS by atom type (top) and the partial (PDOS) orbital breakdowns below for (a) Pr_3RuI_3, (b) Gd_3MnI_3, and (c) Pr_3RuCl_3.

large separations, 4.18 Å. In retrospect, the operation of certain matrix effects here can be imagined in which the large Pr and Ru atoms and closed-shell I····I repulsions all serve to restrain or prevent the additional bonding that is realized in the two following compounds. This condition could even be inferred according to the average Pr−Ru and Pr−Pr contact distances, which differ from standard single-bond metallic radii sums[23] by ∼ −0.08 and +0.65 Å, respectively. The structure of the corresponding chloride (below) also supports the idea of important nonbonding repulsions in the iodide, but other structural differences also enter in.

Descriptions of such products have commonly focused on the metal clusters. These date back to the simple (rather than stuffed or condensed) cluster halides of Nb, Ta, Mo (e.g., Ta_6Cl_{15}),[24] characteristics that were later extended to include the electron-poorer, isolated zirconium cluster halide analogues, which all evidently require additional interstitial (*Z*) atoms for stability. Accordingly, structural drawings of the predominant centered clusters in these and the many reduced rare-earth metal examples that followed have commonly emphasized the formation of clusters by means of lines or "bonds" drawn between the R atoms, these serving to guide the eyes geometrically if not to ratify the R−R-bonding basis for the structures, as in Figure 1. (von Schnering's special spectacles for recognizing clusters[25] can be very helpful.) Important electronic contributions from intermetallic R−Tn bonding in these were recognized early,[17] but this feature has largely been described only in reference to Brewer's thermochemical evidence for strong, polar, early−late transition metal bonding,[18] whereas the R−X interactions have frequently been judged as (fairly) "ionic". Limitations of earlier Extended Hückel analyses of such bonding features have also become more evident following numerous analyses of electron-poor Zintl phases (above) by TB-LMTO-ASA (DFT) methods.[4−10] The greater credibility of such ab initio results have been especially helpful in analyzing complex extended networks in which nominal bond polarities (∼differences in Mulliken electronegativities), high coordination numbers, extensive electronic delocalization, and substantial involvement of d orbitals on Tn are all important. The Crystal Orbital Hamilton Populations (COHP) introduced by Dronskowski and Blöchl[11] and their energy-weighted integrands (−ICOHP) have been especially useful.

Two representations of the atom−orbital−population−energy relationships are used throughout, as shown in Figures 2 and 3 for all three compounds for easier comparisons. The collective densities-of-states (DOS) data for Pr_3RuI_3, also broken down by atom and by orbital types (PDOS), appear in Figure 2a as a function of energy. (All plots are for the primitive cells, *Z* = 2 except for the centered Pr_3RuCl_3, *Z* = 4.) Figure 3a shows the overall COHP values (Hamilton populations; eV) versus energy for each pairwise interaction type in Pr_3RuI_3. (These are reported for all distances up to, but not including, the numerous but relatively unimportant *b* axis repeats, 4.28 Å here.) The partial data generally afford ready approximations regarding the orbital origins within each bond type in the COHP (bonding) data. Thus, the notably broad I 5p and Ru 4d distributions qualitatively correlate well with the energies of the Pr PDOS, not just for 5d but for 6s and 6p as well, roughly accounting for the broad DOS band between −1.5 and −4.7 eV, Figure 2a.

---

(23) Pauling, L. *The Nature of the Chemical Bond*, 3rd ed.; Cornell University Press: Ithaca, NY, 1960; p 403.

(24) Schäfer, H.; Schnering, H.-G. *Angew. Chem.* **1964**, *76*, 833.

(25) von Schnering, H.-G. *Angew. Chem.* **1981**, *93*, 44.

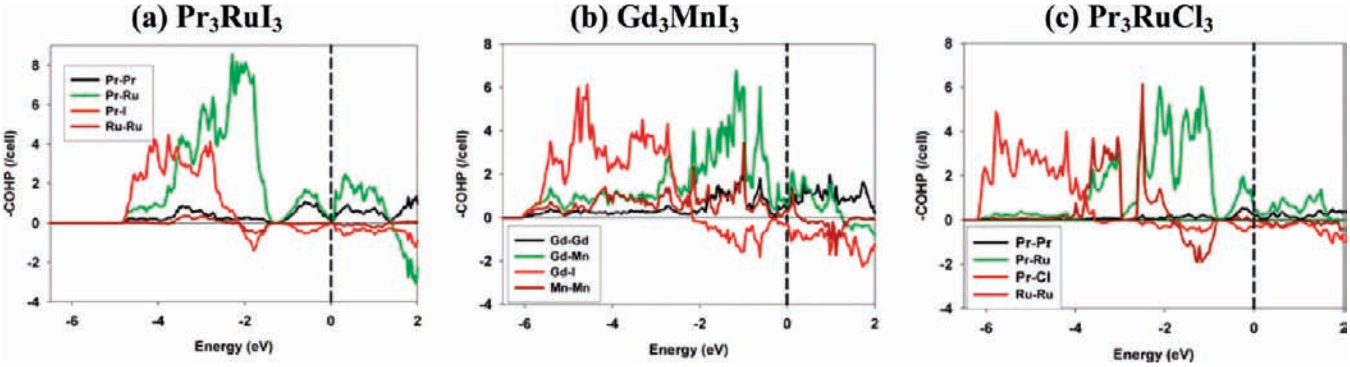

Figure 3. COHP values per cell (eV) as a function of energy for the different pairwise bond types in (a) Pr_3RuI_3, (b) Gd_3MnI_3, (c) Pr_3RuCl_3.

A substantial fraction of the Pr 5d (bonding) states fall above E_F, consistent with valence orbital proportions in the compound and the greater Pr−Ru and Pr−I bonding reflected in the COHP data. The COHP functions, Figure 3a, emphasize the major bonding roles of Pr−Ru (green) and Pr−I (red) and the lesser Pr−Pr contributions (black). The Pr−Ru interactions are distributed over the entire energy region and involve valence d, s, and many p orbitals on both, suggesting significant delocalization of this bonding, in contrast to the simpler polar Pr−I (6p) interactions. The three independent Pr are by no means equivalent, below.

Some significant chemical trends are evident in the DOS data (Figure 2a). Appreciable charge transfer or at least orbital repopulation can be inferred for all three elements. An appreciable fraction of the I 6p states falls below E_F. Likewise, a negative oxidation state for/charge transfer to/additional bonding of ruthenium is implied inasmuch as Ru 5s, almost all Ru 4d, and some of its 5p states lie below E_F, in contrast to its classical $4d^75s^1$ valence configuration. (IDOS values are 0.67, 6.89, and 0.24, respectively.) Correspondingly, the orbital energy distributions for the reducing agent Pr, Figure 2a, clearly reflect its substantial oxidation. Many Pr 6s and 6p states fall below ~ −1.5 eV, whereas, as noted, a significant number of Pr 5d states lie above E_F (10 − IDOS = 8.51), the relative energies of the more penetrating 6s and 6p orbital components falling faster as the metal is oxidized. In fact, the diminished utilization of the R 5d orbitals (or 4d or 3d in Y, Sc compounds) in R−R or R−Tn bonding is a common theme and not only in these polar intermetallics. Indeed, this d-state distribution is a general bonding characteristic between early and late d elements, even in simple binary phases in which the orbital distributions and COHP data likewise qualify them as "polar intermetallics", as in Ti−Fe and Ti−Ru,[26] for example.

Some substantial differences appear among the −ICOHP output for individual Pr−Pr and Pr−Ru contacts. These quickly draw attention to some remarkable yet hitherto unrecognized electronic differences among them, all centered on Pr2, the apical atoms in the double chain (Figure 4). Comparisons of the refined distances with the −ICOHP values for each bond are both listed in Table 1 and marked in Figure 4. The largest contrasts lie between the five independent Pr−Pr distances, which vary only from 3.81 to 3.99 Å (4.5%), their Hamilton populations which vary by a *factor* of 4.5, that is, from two at 0.080 and 0.076 to three at 0.235−0.339 eV/bond·mol. The small populations pertain to Pr1−Pr2 and Pr2−Pr3 contacts, 3.95 and 3.92 Å (two each), in distinct contrast to the large populations for the 3.81 to 3.99 Å separations around the waist of the chain, Pr1−Pr1(×2) and two different Pr1−Pr3 (3 total), Figure 4. This relatively unprecedented disconnect between bond length and "strength" (population or index) evidently originates with some external matrix (bonding) effect[27] that holds the Pr2 vertex in place, close to Pr1 and Pr3 but with a low bonding electron density between them.

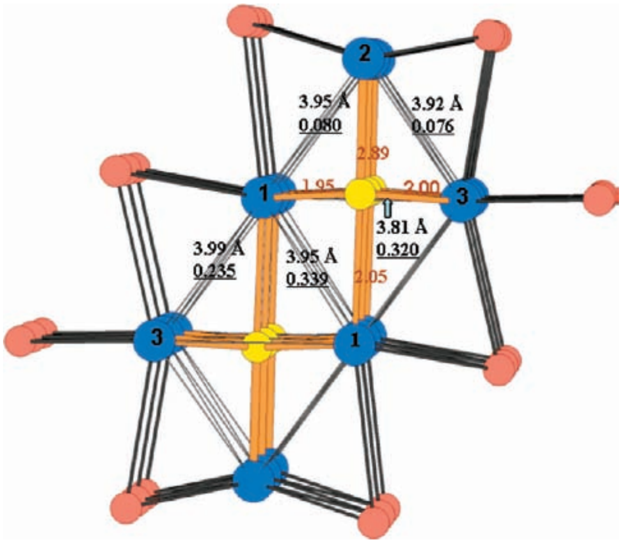

Figure 4. Distances (Å) and −ICOHP populations (eV/bond·mol) in Pr_3RuI_3 for Pr−Pr contacts (black) and −ICOHP data for Pr2−Ru bonds (brown).

Data for the intimately associated Pr−Ru bonding in the chain point to the reason for the foregoing puzzle. Strong Pr−Ru bonding is general, and in this instance the more external Pr2−Ru bond is both remarkably short, 2.571(1) Å, and evidently very "strong", −ICOHP = 2.89 eV/bond·mol. The other five Pr−Ru contact lengths cluster between 2.851 and 2.884 Å, with similar populations between 1.95 and 2.05 eV, namely, Pr1−Ru (×2) and Pr3−Ru (×2) in the waist of the octahedron and Pr1−Ru (×1) at the other vertex (Figure 4). The short

---

[26] Gourdon, O.; Gout, D.; Miller, G. J. *Encyclopedia of Condensed Matter Physics*; Bassani, B. S., Liedl, G., Wyder, P., Eds.; Elsevier: New York, 2005; pp 409−422.

[27] Corbett, J. D. *J. Solid State Chem.* **1981**, *37*, 335.

Table 1. Distance (Å) versus −ICOHP (eV/bond·mol) Values for Individual Pr−Pr and Pr−Ru Contacts in Pr_3RuI_3

contact	distance (Å)	−ICOHP (eV/bond·mol)	multipl.	contact	distance (Å)	−ICOHP (eV/bond·mol)	multipl.
Pr1−Pr3	3.807	0.320	1	Pr1−Ru	2.864	2.051	1
Pr1−Pr1[a]	3.949	0.339	2	Pr1−Ru	2.884	1.949	2
Pr1−Pr2	3.955	0.080	2	Pr2−Ru	2.571	2.890	1
Pr1−Pr3	3.997	0.235	2	Pr3−Ru	2.851	2.002	2
Pr2−Pr3	3.915	0.076	2				

[a] Among the *b*-axis repeats that have been neglected throughout, only that for Pr1−Pr1 (4.28 Å) matters, with −ICOHP = 0.135.

Table 2. −ICOHP Results per bond·mol and per Cell (Z = 2, eV) for Pr_3RuI_3, Gd_3MnI_3, and Pr_3RuCl_3[a] and the Percentage Contributions of each Bond Type

pair-wise interactions ("bonds")	distances, Å	aver. −ICOHP (per bond·mol)	number of bonds per unit cell	cumulative −ICOHP per cell[a] /sum	contribution (%)
		Pr_3RuI_3			
Pr−Pr	3.81−3.99	0.198	18	3.56	8.70
Pr−I	3.21−3.49	0.484	24	11.6	28.4
Pr−Ru	2.57−2.88	2.140	12	25.7	62.7
Ru−Ru	4.18	0.027	4	0.11/41.0	0.26
		Gd_3MnI_3			
Gd− Gd	3.66−3.90	0.385	14	5.39	10.5
Gd −I	3.13−3.53	0.732	24	17.6	34.1
Gd −Mn	2.90−3.23	1.447	14	20.3	39.4
Mn −Mn	2.66	2.062	4	8.25/51.5	16.0
		Pr_3RuCl_3			
Pr−Pr	3.65−3.93	0.106[b]	14	1.49	4.3
Pr −Cl	2.88−3.26	0.373	28	10.4	30.0
Pr−Ru	2.74−3.38	1.303	14	18.2	52.5
Ru −Ru	3.08	1.148	4	4.59/34.8	13.2

[a] Pr_3RuCl_3 data are per half cell, Z = 2. [b] 0.096 if the 4.00 Å Pr−Pr edges in the chain are included.

Pr2−Ru actually places Ru slightly outside of the waist of the octahedral cluster defined by Pr1 and Pr2. These strong Pr2−Ru interactions are responsible for the major peak in the COHP plot around −2.0 eV (green, Figure 3a).

This is a more extreme example of the general effects of strong bonding. The source lies with the domination that polar R−Tn and then R−X bonding have on secondary R−R interactions, populations and, sometimes, distances. The Pr2 atom has in effect withdrawn from the weaker homoatomic cluster bonding in favor of the polar bonding components Pr−Ru and Pr−I. Pr2 has the largest number of bonds to iodine, five, with the four marked in the figure (to I2, I3) having among the larger such populations (0.59, 0.47), plus the shortest and the most populated Pr−Ru bond. The neighboring Pr2−Pr-(1,3) distances in effect reflect more the large sizes of these atoms, but with a considerable exclusion of bonding electron density in the intervening regions. Correspondingly, the Wigner−Seitz sphere radius for Pr2 is the smallest, 1.56 Å versus 1.90 and 1.85 Å for the other two Pr, and it contains the smallest valence electron count (QVAL) among the three, 1.40 versus 2.85 (Pr1) and 2.31 (Pr3) up to the Fermi energy. This then is the most oxidized of the three Pr. (QVAL for the other atoms are Ru, 7.80; I1 (major bridging between chains), 5.03; I2 (3-bonded to Pr), 4.85; I3, 5.26.) Again, note how prominent, even excessive, is the role that distances commonly play in interpreting or cataloging structures, particularly for the more complex and condensed examples.

A separate band of modest dispersion appears in the Pr_3RuI_3 DOS between −1.3 eV and the small gap at E_F (Figure 2a), corresponding to the last two of the 32 valence electrons per formula unit involved in active bonding. The PDOS in this region are principally Pr 5d, although the COHP bonding data indicate that Pr−Ru interactions make a somewhat greater contribution to the bonding population here (Figures 2a and 3a). All Pr−Pr COHP values involving Pr2 interactions are very substantially less than for other Pr, not only here but also across the entire band at lower energies. Examinations of the orbital coefficients across the top band show that the larger terms involve d_{xz} and $d_{x^2-y^2}$ orbitals on Pr1 and Pr3 together with only smaller p_x and p_z coefficients on Ru, that is, at the top of its bonding orbitals. The p_x orbital coefficients on I1 (the interchain bridge) are comparable to the first in size but are antibonding (lone pairs).

We have also been reassured that this unusual Pr_3RuI_3 result does not originate from promulgation of a typographical error, for example, in the published coordinates for the Ru atom. A 2001 report on the bonding in a larger series of distorted R_3RuI_3 phases[28] also included refinement data for the isostructural La_3RuI_3. This exhibits very similar distortions; the difference between the La-(apex)−Ru distance and the average of the others is just 0.010 Å less than here. The next possibility, Gd_3RuI_3, is instead distorted toward the prototype Gd_3MnI_3, below.

Finally, −ICOHP data up to E_F for each bond type in all three compounds are collected in Table 2 for an overall view. The ranges of distances and the average, energy-weighted −ICOHP values per bond·mol are listed in

---

(28) Köckerling, M.; Martin, J. D. *Inorg. Chem.* **2001**, *40*, 389.

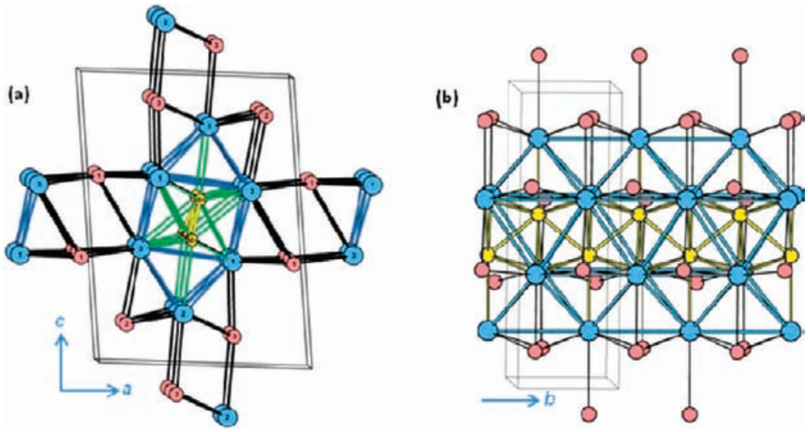

Figure 5. ~[010] and [100] projections of the structure of Gd_3MnI_3 ($P2_1/m$). (Additional chains are centered at the corners of the cell.) (a) The two condensed chains of alternating octahedra in the parent structure (Figure 1) have shifted laterally along *a* with a gain of Mn−Mn and Mn−Gd bonding. (b) View along *a* of a section of one chain and its bonded iodines. Note that that the centered octahedra still alternate in depth along *b*, but lie in a nearly common plane in that projection. (Gd is blue, Mn yellow, and I light salmon.).

columns two and three. The total −ICOHP bond indexes for each type, column five, follow according to the numbers of bonds of each type in the unit cell (column 4; $Z = 2$). Finally, the last column lists the percentage population contributionfor each bond type in each phase, these allowing relatively simple intercomparisons as to which bond types are particularly important (or not) among the different components and structures. The relative magnitudes of the individual −ICOHP bond population data in Pr_3RuI_3 are not greatly perturbed by the different frequencies among bond types. The cumulative population data roughly parallel the areas under the −COHP curves, Pr−Ru > Pr−I > Pr−Pr > Ru−Ru, Figure 3a, which lack the energy-weighting of the former. The dominance of the polar Pr−Ru (≈ 5d−4d) interactions is particularly striking, a characteristic anticipated in general terms by Brewer and Wengert,[18] and this is followed by ~45% as large a contribution from twice as many Pr−I contacts. Compared with the other examples to follow, the large Pr−Ru population here apparently arises from the lack of competition from Ru−Ru bonding because the Ru interstitials are well separated (4.18 Å). The anomalies with Pr2 bonding would be difficult to anticipate from just the structural data, but their effects are explicit in the LMTO output for the independent bond types (Table 1).

The results in Figures 2a and 3a are appreciably different from those from 1992 EHTB−COOP analyses of a single chain in Pr_3RuI_3.[19] the result of which is reproduced in Supporting Information, Figure S2. However, both are in agreement with a (pseudo) closed shell result at 32 active valence electrons, which in the earlier instance arose from an empirical 14-electron metal−metal-bonded core model plus $(5p^6)_3$ closed shells for iodine. The effects of Pr oxidation can (with some hindsight) be recognized in the older data as well, noting that this calculational method does a poor job of modeling R states above E_F. The present results feature decidedly broader PDOS bands and larger bond populations for all atom/bond types. Notwithstanding, these population trends are not those that might be expected qualitatively according to just conventional geometric representation of the structures, as in Figure 1. As we have seen, connections ("bonds") customarily shown between neighboring atoms in a structural drawing are not nearly as uniform in effect. Rather, these "framework bonds" more often serve to guide the eye and to impart a more geometric understanding of the structure. These renditions often communicate distances as well, but these may be only be fair approximations to degrees of bonding, especially in compact, polar and more delocalized situations.

Gd_3MnI_3. This phase, discovered in 1994 well before its time,[20] now fits into a fairly regular series in terms of structural distortions and COHP populations. Its structure, Figure 5, can be directly derived from that of Pr_3RuI_3, Figure 1, through sizable concerted displacements of the two metal chain portions within the *ac* plane in the same $P2_1/m$ space group. These increase the numbers of R−Tn (Gd−Mn) and Tn−Tn (Mn−Mn) bonds, with some decrease in the number of Gd−Gd contacts. Intrinsic differences in atom sizes and bonding characteristics are thought to be important. However, this distortion does not result in a cluster merger, as Figure 5a might imply; the two chains only move into a more nearly common plane in this view, but the alternating depths of the polyhedra along *b* are retained, Figure 5b.

Relative to Figure 1, the displacements give each Mn one more (seven) Gd neighbor in 1:4:2 polyhedra (unicapped trigonal prisms J49[29]), which alternate in orientations in projection along *a* to generate condensed chains, Figure 5b. The yellow interstitial atoms (Ru → Mn) have moved toward each other by about 1.5 Å so as to generate a clear zigzag chain (d(Mn−Mn) = 2.66 Å) along the short *b* axis. The sheathing iodines follow the distortions of the metal core quite well, with no changes in functionality. (A further series of isostructural phases with distorted Tn chains that lie in-between those in Figures 1 and 5 have been found in a wide R_3RuI_3 series, the distortion increasing over R = La, Pr, Gd, Y, Er and, at the extreme, in $Gd_3IrI_3 < Y_3IrI_3$, but none of the Tn−Tn distances in these falls below 3.14 Å versus 2.66 Å here for Mn and 3.08 Å in Pr_3RuCl_3, below. The distortions within the narrower R_3RuI_3 group were later analyzed in terms of increased mixing between R and Ru valence orbitals.[28])

Both Gd and Mn are conventionally considered to be a little smaller than Pr and Ru, respectively, and Mn has

---

(29) Alvarez, S. *Dalton Trans.* **2005**, 2213.

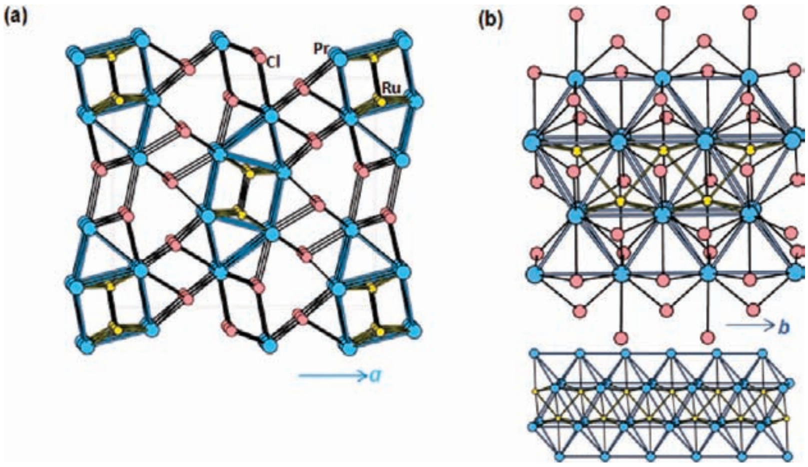

Figure 6. Representations of the structure of Pr_3RuCl_3: (a) Projection of the unit cell along the short *b* axis (*Pnma*) in which adjacent rows of bimetallic chains along *c* (vertical) in Figure 5 have in effect been displaced ~c/2, reflected in alternate directions, and converted to a rectilinear cell. On the other hand, the internal Pr−Ru structure remains very similar to that in Gd_3MnI_3. This distortion appears to be a clear consequence of increased Pr−halide bonding at the metal chain vertices. (Compare the interchain halogen bridging motif at the top and bottom of each chain in (a) with that in Figure 5(a).) (b) Side [100] views of a single metal chain with (top) and without (bottom) the bonded chlorine atoms (see text).

one fewer valence electron per mol (−3% in valence electrons). The larger R−R dimensional changes from Pr_3RuI_3 amount to (1) ~ 0.2−0.3 Å decreases in most R−R bond lengths, and (2) a 0.15 Å decrease in the repeat distance along the chains (*b*), but these are secondary. The various *d*(R−I) decrease by < 0.1 Å, more appropriate to just the difference in standard cationic crystal radii (0.07 Å).[30] The R−Tn distances around the chain center, Figure 1a, (~2.9 Å) increase slightly during the Ru to Mn transformation, whereas the Tn displacement leads to an increase in its distance to the opposed R apex by over 0.5 Å, but a seventh (3.23 Å) Gd−Mn interaction is gained across the double chains. Dimensionally, major factors in this remarkable structural change are gains of two Mn−Mn and four Gd−Mn bonds per cell, both with major d−d orbital contributions, but without a change in Gd−Gd contacts.

Notwithstanding, these dimensional implications are not as meaningful or useful as changes in DOS distributions and relative COHP population indexes. (In the same vein, distances for the five independent Gd−Mn interactions *do not* order well with respect to the −ICOHP values, Supporting Information, Table S1, reminding us of the general lack of a relationship between bond population (electronic distribution) and distance in such situations.) The DOS and PDOS data, Figure 2b, are somewhat similar to those for Pr_3RuI_3 except that the overall width of the occupied states has increased appreciably; the Mn 3d and Gd 5d (mainly) valence states are narrower and higher, and the iodine p band is broader and lies about 1 eV lower. The fraction of R 5d states that fall above E_F has increased appreciably from that in Pr_3RuI_3 and lie even higher. Both appear to originate from stronger and more polar R−I bonds (below). An appreciable number of Mn 3d states now fall above E_F too, a new feature among Tn.

Again, the clearest assessment of the changes appears in the corresponding COHP data as a function of energy and bond type, Figure 3b. A principal difference from Pr_3RuI_3, in which Pr−Ru bonding is dominant, is that the Gd−Mn equivalent has narrowed and moved to higher energy, appropriate to both elements' smaller ionization energies. This gives less competition to Gd−I, and an increase in its COHP at lower energies is obvious. Variations in −ICOHP data can now be anticipated pretty well, Table 2. An evidently improved mixing of valence orbitals (and a lack of bonding aberrations as found in Pr_3RuI_3) afford a somewhat larger Gd−Gd contribution per bond, and the less perturbed R−I bonding translates into a ~50% larger −ICOHP value for Gd−I relative to that for Pr−I. On the other hand, the major fractional contribution of the intermetallic R−Tn network in the former has decreased appreciably, whereas the Mn−Mn interactions that are so evident in the structure are still a relatively small fraction of the total −ICOHP (~16%) because of their infrequency. The net is that polar Gd−I and Gd−Mn populations (bonds) now constitute 34 and 39% of the total Hamilton populations for this compound, the former showing the effects of what can be considered an increased polarity. We do not have the advantage of knowing other examples of this structure type.

Pr_3RuCl_3. The recently discovered Pr_3RuCl_3[21] crystallizes in orthorhombic *Pnma*, which is the maximal non-isomorphous supergroup of $P2_1/m$, with four rather than two formula units per cell, Figure 6. The structure can be redescribed in terms of substantially the same local *metal* chain structure as in Gd_3MnI_3, including the same symmetry elements: 2-fold screw axes along the chain, mirror planes normal to *b*, and the inversion centers on the Tn−Tn midpoints. The additional screw axes and other operations of the higher group all lie between the metal chains. The major change is that 20% more chlorine atoms are bonded to the bimetal chain than in either of the iodides, principally because longer range I···I nonbonding (closed shell) interactions restricted the bonded halogen densities in the chain iodides.. This difference is clearly implied by the magnitudes of the shortest interhalogen distances, ≥ 3.42 Å for Cl···Cl in Pr_3RuCl_3 versus ≥4.02 Å for I···I in Gd_3MnI_3 and ≥4.18 Å with the larger metals in Pr_3RuI_3, with inter-halogen frequencies of 1-2, 6, and 8 contacts per halogen, respectively. The chain

---

(30) Shannon, R. D. *Acta Crystallogr.* **1976**, *A32*, 751.

packing is most constrained in Pr_3RuI_3 whereas the smaller Gd and Mn components allow additional bonding with no changes in halogen bridging functions. The smaller chlorine results in a redistibution of bonds and bonding, but not always in simple and predictable ways when these parameters are intercompared (below).

Figure 6a shows the newer chloride structure in a [010] projection along the chains ($b = 4.00$ Å), and Figure 6b, a [100] side view of a single chain, in parallel with similar views of Gd_3MnI_3 employed in Figure 5. The second view is as the structure was originally described,[21] unicapped trigonal prisms with alternate orientations along $\pm c$ that share pairs of side faces to generate the condensed zigzag chain along *b*. The additional processes that lead to gains in the number of Pr−Cl bonds relative to those in the Gd−I and Pr−I patterns can be visualized qualitatively via a series of fairly simple changes that convert the monoclinic structure, Figure 5a, into the higher symmetry orthorhombic Pr_3RuCl_3 (*Pnma*) with twice the volume, Figure 6a. The increased R−X bonding in the chloride occurs mainly in the underbonded region around the isolated face-capping (3-bonded) iodines at the upper right and lower left of the chain, Figure 5a. A new herringbone pattern of chains is formally obtained from the Gd_3MnI_3 structure after every other row of chains parallel to *c* (vertical) in the *b* projection is both displaced by $c/2$ and reflected along *a*. (The 96° β angle is also reduced to 90°.) The opposed tilt of neighboring chains in the modified rows puts additional chlorine into the so-described underbonded region (and vice versa), so that, with some smaller rearrangements, a more uniform interchain bridging motif is obtained all around the chain. The chains now have 12 interchain halogen bridges around their circumference compared with ten before. (In effect, the halogens in Figure 5a are rotated clockwise around the chain during this transformation except that the reference interchain R−X bridges at the top and bottom R vertices in the former are retained but become bent.) The more nearly uniform bonding pattern all around the chains leads to an average increase of two in the chlorines bonded to each R.

Not surprisingly, these displacements and the tighter bonding produce other changes in the geometric details of the $(R_3Tn)_2$ chains, particularly an elongation of (the weaker) waist R−R distances along *c* by ~0.2 Å. Other internal features of the metal chains remain about the same. However, the important R−Tn interactions generally decrease about 0.25 Å in spite of an ideal expectation that Pr and Ru atoms are larger than Gd and Mn, respectively. In fact the entire bonding system is different.

The side view of the chloride-sheathed chain in Pr_3RuCl_3, Figure 6b, illustrates first the great similarity of the blue−yellow metal framework alone to that in Gd_3MnI_3, Figure 5b. But second, sizable displacements of some halogen positions on the present chain accompany the rotative distortions and gains in the number of R−X bonds, giving distinctively different halogen patterns in the two [100] views. The lower inset in Figure 6b emphasizes the common bimetallic chain structures in the two; a more detailed comparison of these is given in the Supporting Information, Figure S2.

The DOS, PDOS, and −COHP results for Pr_3RuCl_3 are in Figures 2c and 3c, and its individual and total −ICOHP values are listed in the bottom portion of Table 2. (To be consistent, the last are expressed in terms of the same two formula units as the iodides.) Relative to the Gd−Mn phase, the Pr−Cl and Pr−Ru COHPs both lie lower in energy, Figure 3, and are better separated. The latter contributes a significantly larger fraction of the total bonding too (−ICOHP). The Ru−Ru COHP band falls in an intermediate position, somewhat lower than for Mn, and it is admixed with Pr−Ru bonding over ~ −3.8 to −2.0 eV, suggesting delocalization in a more common bonding. The Ru−Ru band contribution becomes antibonding in the higher portion. The further redistribution of R 5d states is striking. Only one small Pr−Pr band remains just below E_F, and an even greater fraction of the R states lie above E_F (Figure 3c and at higher energies), evidence of greater oxidation of Pr via the electron-withdrawing Cl and Ru. Even more striking evidence of bonding redistribution between the more closely related end members Pr_3RuI_3 and Pr_3RuCl_3 is seen in the COHP data, Figures 3a versus 3c. Both the relative Pr−Pr and the dominant Pr−Ru bond populations fall appreciably in the chloride (Table 2), for which the appearance of new (but few) Ru−Ru interactions and more Pr−Cl bonds would appear responsible.

Many of the bonding effects and trends for all three compounds can be found among the −ICOHP data summarized in Table 2 on a common basis of two formula units, but it must be remembered that these R_3TnX_3 subjects contain different elements and several structural differences. But numerical differences between phases should be considered with care. Changes in the frequency of the four bond types are meaningful from the viewpoint of structural stability, but all of the −ICOHP data are intrinsic to particular compounds, from individual bond averages to the sums of all the components for each phase. The closer structural comparison between Pr_3RuI_3 and Pr_3RuCl_3 data shows particularly well how Pr−Pr bonding in the homoatomic framework in both is quite insignificant in terms of total Hamilton bond populations, decreasing from ~8% to ~4%. On the other side, the polar 5d−4d bonding between the early−late Pr−Ru metals amounts to over 50% of the total −ICOHP in both examples, although the overall results are surely affected by either negligible Ru−Ru competition in the iodide or the enhanced numbers of Pr−X and Pr−Ru bonds in the chloride. In general, the R−Tn host−interstitial terms are the dominant contributors in all three phases, and the polar R−Tn plus R−X components constitute 75 to 90% of the total populations. Although the individual Tn−Tn contributions are relatively small in both Gd_3MnI_3 and Pr_3RuCl_3 (~15%) because of their infrequent occurrences, their roles as new bonds in the structures are obvious. The relative magnitudes of the Hamilton populations for what we label as the polar intermetallic R−Tn bond types are certainly supportive of the enhanced thermochemical stabilities first reported or predicted for comparable early−late transition metal compounds by Brewer and co-workers in 1973.[18]

Elsewhere, these general bonding insights would certainly pertain to the closely related Pr_4TnI_5 compounds, Tn = Co, Ru, Os,[22] which contain similar but single chains of edge-sharing Pr octahedra centered by Tn and wrapped with iodine. However, a large majority of all other centered cluster halides are distinctly halogen richer, and their structures contain only separate halogen-interbridged

R_6TnX_{12}-type cluster units. Although these lack longer-range delocalized bonding and are doubtlessly all poor semiconductors or insulators, their internal cluster bonding must still feature a corresponding dominance of polar R−X and R−Tn components. On the contrary, a more condensed group of R_xTn tellurides with new and distinctive structural features result when roughly half as many monotelluride anions are substituted for halide.[13,14] Numerous examples contain sheets or 3D networks built of condensed Tn-centered tricapped trigonal prisms of R, with telluride bound among or between these. Only one has been studied by such ab initio means, $Er_7Au_2Te_2$,[31] principally to examine the degree to which scalar relativistic effects that are particularly important for gold bonding in derivatives of the electron-poor/metal-rich Zintl phase analogues (below) also persist in the rare-earth-metal counterparts. The gold again expresses a high effective electronegativity, and the Er−Au Hamilton population is 49% of the total −ICOHP versus 37% for Er−Te and only 14% as Er−Er, in spite of the 64 at. % Er content of the compound. The three COHP components are well separated, and Te 6p and Au 5d, 6s, and most of the Au 6p PDOS states are filled at E_F, again leaving Lu relatively well oxidized.

The present three compounds were selected from among a number of ternary R−Tn−X phases because of the relative simplicity of their lower dimensional bonding and (presumed) metallic conduction inasmuch as these features would enable better comparisons with the bonding in the converse family of relatively electron-poor "polar intermetallics". The latter are often described as electron-poor Zintl phases made up of an active metals, primarily from groups 1−3, and a countervailing polyanionic group, often a late transition metal and an early p-metal. The role reversal here is clear; the active metal atoms are separate, particularly the alkali-metals, whereas the alkaline-earth metals are commonly singly encapsulated in the mixed metal anionic networks, not unlike the counter role of telluride. The heavy transition metal components, Au especially, have been found to dominate in this class of intermetallics in terms of both structural variety and bond populations, forming strong polar bonds with the later triel or tetrel (group 13 or 14) metals, particularly in the presence of alkali-metal cations A^+. So far, the relationships of the last to those in the "inverse" type of compounds considered in this article appear to be only rather general, but the diversity of structures and bonding within the whole collection of polar intermetallics and related "salts" is large and stimulating.

One of the problems that stimulated this study remains unresolved: the distant or even contradictory relationships between the customary "ball and stick" structural representations and significant bonding features in these structures, particularly now that the latter can be well approximated by creditable calculations accessible to experimentalists. One idea, to use variable line *widths* for the interatomic connections to code two-center bond population weights among the different types, is probably not very useful if it diminishes the general "understanding" of the structure itself. "Structural" drawings intended to guide the reader regarding both geometric features of the structure and dominant bonding effects are probably too much to ask. Nonetheless, common structural representations of extended solids probably mislead many experimentalists, particularly if superimposed distances are taken as good relative measures of bonding. In these cases parallel bonding analyses can be valuable, even vital, to "understanding" the structural chemistry more broadly and deeply.

Acknowledgment. The authors thank Gordie Miller for his advice and insights on several matters during this venture, including the need for spin-density calculations. This research was supported by the Office of the Basic Energy Sciences, Materials Sciences Division, U.S. Department of Energy (DOE), and was carried out in the facilitates of the Ames Laboratory. The Ames Laboratory is operated for the DOE by Iowa State University under contract No. DE-AC02-07CH11358.

Supporting Information Available: A pictorial comparison of the metal chains in Gd_3MnI_3 and Pr_3RuCl_3; 1992 EHTB results for Pr_3RuI_3; distance− ICOHP comparisons for individual Gd−Mn bond types in Gd_3MnI_3; calculational details. This material is available free of charge via the Internet at http://pubs.acs.org.

---

[31] Gupta, S.; Corbett, J. D. *Dalton Trans.* **2010**, *39*, 6074.